Process Safety and Environmental Protection 182 (2024) 1072–1085

Contents lists available at ScienceDirect

Process Safety and Environmental Protection

journal homepage: www.journals.elsevier.com/process-safety-and-environmental-protection

Modeling the behavior of LPG tanks exposed to partially engulfing pool fires

Giordano Emrys Scarponi *, Valerio Cozzani, Giacomo Antonioni, Ferruccio Doghieri

LISES – Laboratory of Industrial Safety and Environmental Sustainability, DICAM - Department of Civil, Chemical, Environmental and Material Engineering, University of Bologna, via Terracini 28, 40131 Bologna, Italy

ARTICLE INFO

Keywords:
LPG
Storage tank
Partial fire engulfment
Pressure vessels
CFD modeling
Thermal stratification
Digital twin

ABSTRACT

Accident scenarios leading to full or partial fire engulfment represent a serious threat to tanks used for the transportation and storage of dangerous goods. The present study focuses on the impact of partial engulfing fire scenarios on an LPG tank. An experimentally validated CFD modeling approach was further developed and applied to perform a parametric study by varying the exposure mode and the filling degree. The results of the simulations show that both these factors have a strong influence on the pressurization rate, the energy accumulation, and the high-temperature mechanical weakening of the tank structure. Fire scenarios where the flame zone is at the top or at the end of the tank are particularly critical when the liquid filling degree is low or medium. Liquid thermal stratification is evident in all the case studies analyzed and, in most of them, it strongly affects the vessel pressurization curve. The comparison to the results obtained using a lumped model showed that this provides non-conservative pressurization results for high filling levels (80%). The results show that a validated CFD approach can be used as a virtual workbench to support tank design within a digital twinning approach.

1. Introduction

Fire exposure may occur according to different mechanisms, such as full or partial fire engulfment, radiation with no direct flame contact, and jet fire impingement (Ricci et al., 2021). Tank failure may lead to extremely severe consequences (Mannan, 2012). In particular, exposure to fire of fixed and mobile storage tanks is a recurring underlying factor of severe industrial domino accidents (Reniers and Cozzani, 2013). Thus, understanding and predicting the behavior of tanks exposed to fire is paramount to improving the design of fire protection and emergency depressurization systems, ensuring the robustness of quantified risk assessments of industrial activities, and supporting informed decision-making by rescue teams.

As documented in the extensive reviews by Moodie (1988) and Birk (2006), numerous experiments at small, medium, and large scales were carried out in the last decades, especially on LPG tanks. More recently, fire tests were carried out on cryogenic tanks e.g. (Kamperveen et al., 2016); van Wingerden et al., 2022) due to the increasing interest in the storage and transportation of liquefied natural gas and liquid hydrogen. The outcomes of experimental campaigns allowed the identification of the key physical phenomena governing the thermo-hydraulic response of tanks during fire exposure (Aydemir et al., 1988) and supported the development of models for the prediction of tank heating, pressurization, and time to failure (Scarponi et al., 2022). CFD-based approaches were proven to provide results in good agreement with experimental measurements. However, due to the high computational resources required to run them, lumped models (based on the solution of energy and mass balance equations in the integral form) are still the preferred tool by practitioners. The main drawback of the latter models lies in the need to rely on adjustable parameters and simplifying assumptions, which limits their applicability to specific regions where validation was carried out.

To date, most of the experimental and numerical studies (encompassing both CFD and lumped parameter-based approaches) available in the literature focus on full engulfment fire scenarios, and only a limited number of studies investigate tank behavior under localized fire exposure conditions (Birk et al., 2006; Scarponi et al., 2021, 2018b; Wang et al., 2022a, 2022b, 2023). Nonetheless, the latter is often more representative of realistic fire accident scenarios. An example of such partial engulfment scenarios is the recent severe BLEVE event occurred in Italy, where a LPG trailer suffered a road crash that generated a poolfire partially engulfing the tank and leading to its catastrophic

* Corresponding author.
E-mail address: giordano.scarponi@unibo.it (G.E. Scarponi).

https://doi.org/10.1016/j.psep.2023.12.048
Received 3 November 2023; Received in revised form 8 December 2023; Accepted 20 December 2023
Available online 22 December 2023

failure after about 8 min of exposure (Malm, 2018). A symilar dinamyc characterized two accidents that took place in Spain involving LNG tankers, which collapsed (causing a BLEVE) after being exposed for a few minutes to a pratially engulfing pool fire originated from the collision with other vehicles (Planas et al., 2015; Planas-Cuchi et al., 2004). In 2011, a BLEVE was recorded at the Chiba refinery near Tokyo (Japan), as a result of the catastrophic failure of a LPG sphere that was partially engulfed by a massive jetting liquid propane fire from a failed pipeline nearby Japan (Birk et al., 2013).

The phenomena characterizing the thermo-hydraulic response of pressure vessels to fire exposure are complex and interactive. Thus, predicting pressurization (and ultimately time to failure) is a demanding task, that is even more challenging when non-uniform fire conditions are analyzed, due to the important role that local effects come to play. In partial engulfment scenarios, the role of thermal stratification in the liquid phase is of particular importance (Aydemir et al., 1988; Birk and Cunningham, 1996). Stratification is caused by the accumulation beneath the liquid-vapor interface of the fluid heated in contact with the vessel shell regions heated by the fire. Although experiment tests are often considered the most robust approach to assess a specific scenario, the scale-up of partial engulfment fire tests is problematic. In addition, full-scale tests are expensive, time-consuming, and pose relevant safety and environmental issues. The inherent variability of fire conditions in large-scale experiments represents an additional challenge when the comparative analysis of multiple scenarios is of interest. An alternative strategy to overcome this problem is the use of a CFD model, validated using a limited number of full-scale qualified data, to explore vessel behavior over a wider region of conditions and scenarios.

In the present study, the potential of such an approach is explored, carrying out a detailed parametric analysis of partial engulfment fire scenarios, aimed at improving the understanding of how pressure tanks behave in partial engulfment fire scenarios. A validated CFD approach is used to investigate how different exposure modes and degrees of filling affect the thermo-hydraulic response of an LPG tank. Simulation outputs are analyzed to understand how local flow field characteristics promote thermal stratification, driving the pressure build-up. A comparison to the results obtained using a widely adopted zone model available in the literature is carried out, evidencing the conditions in which this simplified approach may produce non-conservative results. The ultimate ambition of the present study is to provide a practical demonstration of how CFD simulations may be considered a “digital twin” of a fire test and can be used to investigate in detail specific aspects that are of interest from the safety standpoint.

2. Numerical model

2.1. Governing equations

The present study follows the CFD modeling approach proposed by Scarponi et al. (2021), which was validated against the experimental data from partial engulfment fire tests on a 500 gal (1.9 m^3) propane tank carried out by Birk and co-workers (Birk et al., 2006). A summary of the validation study, demonstrating the capability of the model to reproduce the pressurization rate and the lading temperature distribution measured during this test is reported in the Appendix. Further details can be found in Scarponi et al. (2021). Simulation results presented in previous studies based on a similar approach proved to be in good agreement with pressurization and temperature data from fire tests considering full engulfing pool fire conditions (Scarponi et al., 2019) and radiation from a distant source (Scarponi et al., 2018b). The CFD setup considered in these studies was further developed to allow for the simulation of different partial engulfment scenarios and advanced post-processing procedures were applied to analyze the key phenomena characterizing the tank response.

The model was implemented using ANSYS Fluent 18.2. The governing equations for the transient, turbulent, multiphase problem involving heat transfer and phase change, mostly based on those adopted in the original model by Scarponi et al. (2021), are reported in Table 1. The *k-ω* SST model was adopted for turbulence, while the Volume Of Fluid (VOF) model (Hirt and Nichols, 1981) and the evaporation-condensation model proposed by Lee (1979) were considered to simulate the two-phase fluid in the tank.

The VOF model was applied to simulate the flow of two (or more) immiscible fluids by solving a single set of momentum equations and tracking the volume fraction of each of the fluids throughout the domain. The phases share the same temperature and velocity field (i.e., in a given cell of the domain, the temperature and the velocity are the same for each phase). The same applies to the turbulent quantities (i.e., turbulent kinetic energy, turbulent specific dissipation rate, and turbulent viscosity). The tracking of the interface between the liquid and the vapor is obtained by the solution of a continuity equation for the volume fraction of the liquid (E01 in Table 1). The vapor fraction is obtained as the complement to 1 of the liquid fraction (E02 in Table 1). The contribution of internal radiation is neglected in the model.

Pure propane was assumed as the operating fluid and its physical properties were expressed as a function of temperature as reported by Liley et al. (1999). The Ideal Gas equation was used to calculate the vapor phase density. The carbon steel wall density, thermal conductivity, and heat capacity were derived from European standard EN 10222-1 (CEN - European Committee for Standardization, 1998).

2.2. Definition of initial and boundary conditions for partial engulfment

Zero velocity and thermodynamic equilibrium were assumed as initial conditions. Turbulent kinetic energy and specific dissipation rate were initialized to 10^{-9} m^2/s^2 and 10^{-3} s^{-1}, respectively. The no-slip condition was considered set at the inner wall. Where possible (see Section 3), symmetry planes were exploited to reduce the computational cost.

The partial fire engulfment thermal boundary condition was defined, following the approach proposed by Scarponi et al. (2021) and adopted by Wang et al. (2022a, 2022b, 2023), to simulate storage tanks partially engulfed in fire. The outer wall was divided into three zones as illustrated in Fig. 1: “engulfed”, “transition”, and “no flame” zone.

Only thermal radiation was considered as the heat transfer mechanism between the tank wall and the environment. Under the assumption that the heat transfer mechanism between the tank wall and the environment (flame and/or air) is purely radiative (see Scarponi et al., 2021), the heat flux entering the faces of the cells laying on the tank outer wall can be expressed according to Eq. (1).

$$q = \sigma \varepsilon_w \left(T_R^4 - T_w^4\right) \tag{1}$$

where ε_w (assumed equal to 0.9) is the wall emissivity, T_w is the temperature of the outer wall, σ is the Stefan-Boltzmann constant (= $5.67 \bullet 10^{-8}$ W m^{-2} K^{-4}), and T_R is the black body temperature of the radiative source. This changes according to the zones depicted in Fig. 1. In the engulfed zone (red zone in Figure 1), T_R coincides with the black body temperature of the fire (T_F). In the zones far from the flame (gray zone in Figure 1), T_R is equal to the value of the air temperature T_{air}. The engulfed and no flame zones are separated by a transition region (orange zone in Fig. 1) in which T_R decreases smoothly with the distance from the engulfed zone (δ) according to Eq. (2).

$$T_R = \sqrt[4]{T_{air}^4 + \left(T_F^4 - T_{air}^4\right) \bullet \exp\left(-a \bullet \delta^2\right)} \tag{2}$$

The parameter a was set to 115 m^{-1} so that along the perimeter of the transition zone (i.e. at $\delta = \delta_T$ as illustrated in Fig. 1) the exponential in Eq. (2) is equal to 10^{-2}.

Table 1
Governing equations for the transient, turbulent, two phases, model considered in the present work.

ID	Property	Equations
E01	Volume fraction of the secondary phase (liquid)	$\frac{\partial}{\partial t}(\alpha_L\rho_L) + \nabla \bullet (\alpha_L\rho_L \vec{u}_L) = \dot{m}_{V\to L} - \dot{m}_{L\to V}$ ρ_L: liquid density (density ($\rho_L = 60.7/0.275^{[1+(1-T/369.83)^{0.29359}]}$, from Liley et al., 1999); t: time; α_L: liquid volume fraction; $\vec{u}_L$: Reynolds averaged velocity; $m_{V\to L}$: and $m_{L\to V}$: condensation and evaporation liquid phase source terms, expressed as follows: $if \quad T > T_{sat}(p) m_{L\to V} = C_E\alpha_L\rho_L\left(\frac{T-T_{sat}}{T_{sat}}\right)$, $m_{V\to L} = 0 \quad if\ T < T_{sat}(p) m_{L\to V} = 0, m_{V\to L} = C_C\alpha_V\rho_V\left(\frac{T_{sat}-T}{T_{sat}}\right)$ T: temperature; p: absolute pressure; T_{sat}: saturation temperature (saturation curve: $Psat=exp(59.078-3492.6/T-6.0669ln(T)+1.919^{-5}T^2)$, from Liley et al., 1999); C_E and C_C: coefficients (both set to the default value of 0.1 s^{-1}); α_V: vapor volume fraction, ρ_V: vapor density (calculated using the ideal gas equation).
E02	Volume fraction of the primary phase (vapor)	$\alpha_V = 1 - \alpha_L$
E03	Two-phase averaged quantity	$\varphi = \varphi_V\alpha_V + \varphi_L\alpha_L$ Two-phase volume fraction averaged property φ function of liquid and vapor properties (φ_L and φ_V, respectively) where φ can be density ρ, viscosity μ, turbulent viscosity μ_T, thermal conductivity k.
E04	Momentum	$\frac{\partial}{\partial t}(\rho\vec{u}) + \nabla \bullet (\rho\vec{u}\vec{u}) = -\nabla p + \nabla \bullet \left[\mu\left(\nabla\vec{u} + \nabla\vec{u}^T\right) - \frac{2}{3}\mu(\nabla \bullet \vec{u})I\right] + \rho\vec{g} - \nabla \bullet \tau'$ ρ: two-phase volume fraction averaged density; p: Reynolds averaged pressure; μ: two-phase averaged viscosity; g: gravity acceleration; I: identity tensor.
E05	Reynolds stress tensor (introducing the Boussinesq approximation)	$-\tau' = \mu_T\left[\left(\nabla\vec{u} + \nabla\vec{u}^T\right)\right] - \frac{2}{3}(\rho K + \mu_T\nabla \bullet \vec{u}I)$ μ_T: two-phase averaged turbulent viscosity; K: turbulent kinetic energy
E06	Turbulent viscosity	$\mu_T = \frac{\rho K}{\omega}\frac{1}{L}$ ω: Turbulent specific dissipation rate; the definition of L can be found in (ANSYS inc, 2015). K: turbulent kinetic energy
E07	Turbulent kinetic energy	$\frac{\partial}{\partial t}(\rho K) + \nabla \bullet (\rho K\vec{u}) = \nabla \bullet (\Gamma_k\nabla K) + G_K - Y_K$ Γ_K: turbulent Prandtl number for K; G_K: generation of K due to mean velocity gradients; Y_K: dissipation of K due to turbulence. The definitions of Γ_K, G_K, and Y_K can be found in (ANSYS inc, 2015)
E08	Turbulent specific dissipation rate	$\frac{\partial}{\partial t}(\rho\omega) + \nabla \bullet (\rho\omega\vec{u}) = \nabla \bullet (\Gamma_\omega\nabla\omega) + G_\omega - Y_\omega$ Γ_ω: turbulent Prandtl number for ω; G_ω: generation of ω; Y_ω: dissipation of ω. The definitions of Γ_ω, G_ω and Y_ω can be found in (ANSYS inc, 2015)
E09	Energy (fluid domain)	$\frac{\partial}{\partial t}(\rho E) + \nabla \bullet (\vec{u}(\rho E + p)) = -\nabla p + \nabla \bullet [k_{eff}\nabla T] + \Delta H_{vap}(\dot{m}_{V\to L} - \dot{m}_{L\to V})$ E: two-phase Reynolds averaged specific energy; k_{eff}: effective thermal conductivity; λ: heat of vaporization;
E10	Energy (solid domain)	$\frac{\partial}{\partial t}(\rho_s Cp_s T_s) = \nabla \bullet (k_s\nabla T_s)$ T_S: temperature in the solid; k_S: steel thermal conductivity; ρ_S steel density; Cp_S steel heat capacity
E11	Effective thermal conductivity	$k_{eff} = k + \frac{c_p\mu_T}{Pr_T}$ k = two-phase volume fraction averaged thermal conductivity c_p: two-phase volume fraction averaged heat capacity, Pr_T: turbulent Prandtl number = 0.85 (ANSYS inc, 2015)

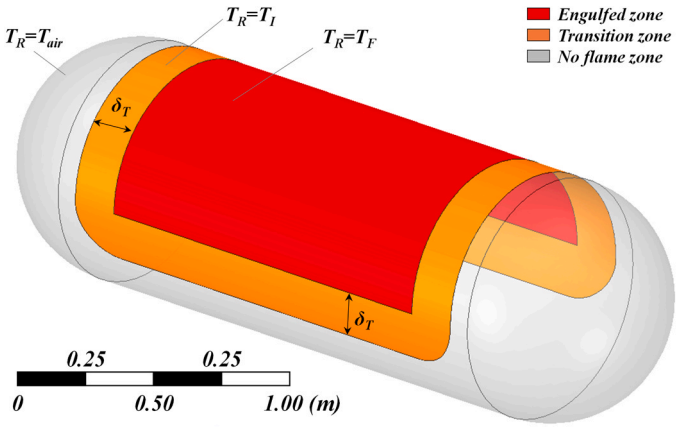

Fig. 1. Illustration of the 3 zones defined to reproduce partial engulfment conditions.

2.3. Solution methods

The second-order upwind discretization schemes were considered for density, momentum, energy, and turbulent quantities (k and ω), while the PRESTO! (PREssure STaggering Option) and Geo-Reconstruction options were selected for pressure and phase volume fraction respectively. SIMPLEC (Semi-Implicit Method for Pressure-Linked Equations - Consistent) was chosen as pressure-velocity coupling algorithm. Gradients were calculated according to the Least Square Cell-Based method. A first-order implicit scheme was adopted for the transient formulation, with a time step of 0.005 s

Convergence was deemed to be achieved, at each time step, when at least one of the residuals-based convergence criteria (absolute or relative) reported in Table 2 was satisfied for every transport equation (ANSYS inc, 2015).

2.4. Computational domain

The computational domain included the fluid inside the tank and the tank wall. Depending on the fire engulfment mode (see Section 3), one of (or both) the symmetry planes illustrated in Fig. 2a was (were) considered to reduce the computational cost. The domain was discretized using the meshing parameters reported in Table 3, which were proved to provide grid-independent results by Scarponi et al. (2021). The resulting grid is a combination of tetrahedral and hexahedral cells, refined near the inner wall region (see Fig. 2b and c), which is characterized by large values of the temperature and velocity gradients.

3. Definition of the case studies

Table 4 reports the list of case studies analyzed in the present work. A total of 15 case studies were defined combining three different filling levels considered for the tank and five different flame "*engulfment patterns*". The "*engulfment patterns*" considered are shown in the first column of Table 4.

As shown in the table, in the first four engulfment patterns, 25% of the tank wall is assumed in contact with the flame, with the engulfed zone positioned respectively on the side (S), top (T), bottom (B), and end

Table 2
Convergence criteria adopted in the present study.

Equation	Absolute criteria	Relative criteria
Continuity	10^{-4}	$5 \bullet 10^{-3}$
Momentum	10^{-4}	$5 \bullet 10^{-3}$
Energy	10^{-7}	$5 \bullet 10^{-3}$
k and ω	10^{-3}	$5 \bullet 10^{-2}$

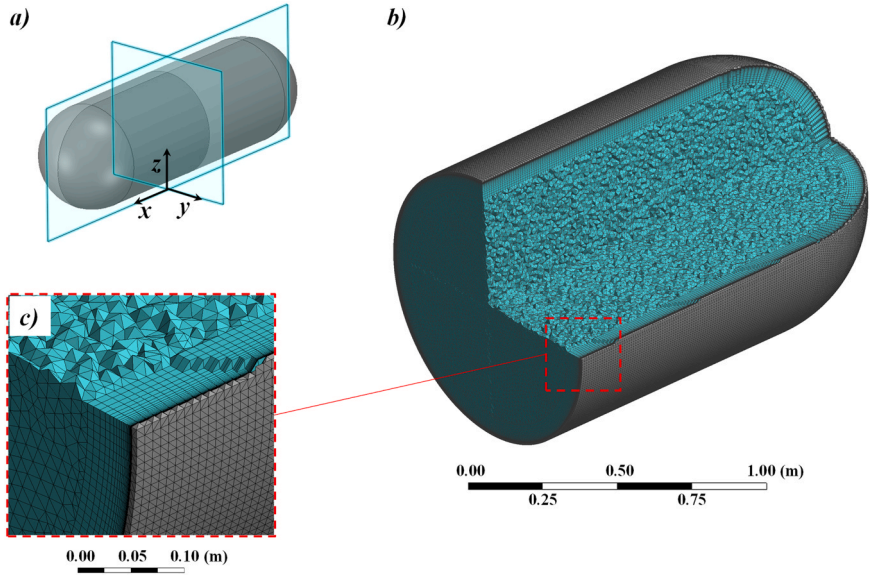

Fig. 2. Computational domain and symmetry planes considered for the CFD simulation (a); overview of the computational grid (b); and (c) detail showing the increased grid resolution in the near wall region (gray and cyan cells refer to the fluid and the solid domains respectively).

Table 3
Summary of the meshing parameters used for the definition of the computational grid.

Meshing parameter	3D
Face size at the inner and outer wall wall (m)	$2 \bullet 10^{-2}$
Maximum edge size (m)	$3 \bullet 10^{-2}$
Growth rate	1.1
Number of inflation layers	25
First layer thickness (m)	$2 \bullet 10^{-4}$
Inflation growth rate	1.2

(E) of the tank.

The engulfment patterns were defined according to realistic exposure scenarios considered in fire tests and in recent accidents: the S and E patterns were tested by Birk and VanderSteen (2006), the B pattern simulates the fire test conditions used by Wang et al. (2022a), (2022b), (2023), while the E and S are representative of the fire scenarios observed in the BLEVE accidents occurred in Italy (Malm, 2018) and in Spain (Planas et al., 2015; Planas-Cuchi et al., 2004) respectively. A full engulfment mode (F) was also considered as a benchmark. The effect of the position of the liquid-vapor interface was analyzed considering the three different filling degrees defined in the case studies: 20%, 50%, and 80% (intended here as the percentage of tank volume occupied by the liquid phase).

In the following, each of the case studies will be referenced using a specific tag obtained combining the engulfing pattern and the filling degree (X_YY%, where YY% is the percent degree of filling and X represents the engulfment pattern mode: S = side, T = top, B = bottom, E = end, and F = full).

The fire black body temperature (T_F) was set to 871 °C, which is the mean value of the range 815 – 927 °C suggested for pool fires by the Canadian General Standards Board (CGSB, 2002), widely used in North America for qualifying tank-car thermal protection systems. For partial engulfment simulations, a temperature of 25 °C was considered for the air surrounding the tank, while the value of δ_T, determining the extent of the transition zone (see Fig. 1), was set to 0.2 m according to the results of a previous study (Scarponi et al., 2021). Thus, the percentage of external wall surface area in the transition zone is equal to 6% or 14% of the total external surface area of the tank, respectively for the end engulfing pattern (E) and for all the other partial engulfing patterns (B, S, and T).

The simulations were carried out considering a 1.9 m^3 bullet tank with hemispherical ends, with an inner diameter of 0.953 m, a wall thickness of 7.1 mm, and a total length (end to end) of 3.07 m. The tank geometrical parameters used in simulations correspond to those of the tank used in partial engulfing fire tests by Birk and co-workers (Birk et al., 2006). In all the case studies, the initial temperature was set to 25 °C. For pure propane, this corresponds to a saturation pressure of 9.52 bar, which was set as the initial value for internal pressure. Simulations were terminated when the tank pressure reached 24 bar, which was assumed as the set point for the pressure relief valve (PRV) opening as in the fire tests carried out by Birk and co-workers (Birk et al., 2006).

4. Results

4.1. Pressure build-up

Fig. 3a reports the pressurization curves obtained for the case studies listed in Table 4. When the degree of filling is high (80%), the influence of the position of the partially engulfed zone is weak, and the pressure rise is generally higher than in the other cases, especially in the first 2 min. On the other hand, large variations in the pressure curves can be observed when the initial filling degree is 20%. Not surprisingly, the top engulfment pattern (T_20%) in this case is the one showing the lowest pressure increase. An intermediate situation is present when the 50% filling degree is considered. When this filling degree is considered, very similar curves were obtained for all the cases where the engulfed zone is positioned on the side (S_50%) and at the and (E_50%) of the tank, while the top (T_50%) and bottom B_50%) engulfing modes result in a slower and higher pressure increase, respectively. As a general consideration, in agreement with pool fire test results available in the literature (Moodie et al., 1988, 1985), the cases with the higher filling degree (80%) showed the most rapid pressurization. Likewise, when the engulfed zone is positioned at the bottom, the pressure increase is faster. These results confirm that the heat transfer to the internal fluid is mostly determined by the portion of the tank surface in contact with the liquid, where the heat transfer coefficient is higher.

Fig. 3b shows the time required to reach a given pressure normalized with respect to the corresponding full engulfment case (F). Although in all the partial engulfment scenarios only one-fourth of the tank surface is exposed to fire, the time to reach a given pressure is between 1.5 and 3

Table 4
Summary of the case studies analyzed. The three last columns of the table report the tag used to identify each case study (S = side, T = top, B = bottom, E = end, and F = full).

		Number of cells	Symmetry plane (s)	Degree of filling		
				20%	50%	80%
Engulfment patterns	Side 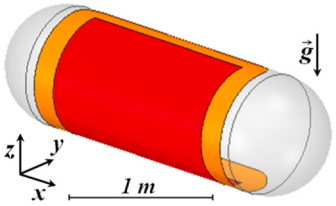	931,088	yz	S_20%	S_50%	S_80%
	Top 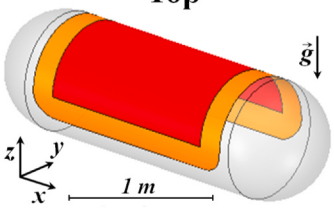	931,088	yz	T_20%	T_50%	T_80%
	Bottom 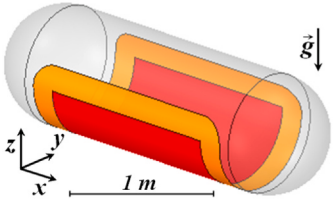	931,088	yz	B_20%	B_50%	B_80%
	End 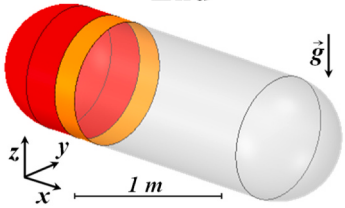	775,828	xz	E_20%	E_50%	E_80%
	Full engulfment 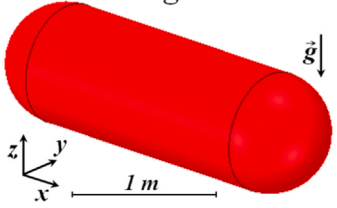	451,982	xy, xz	F_20%	F_50%	F_80%

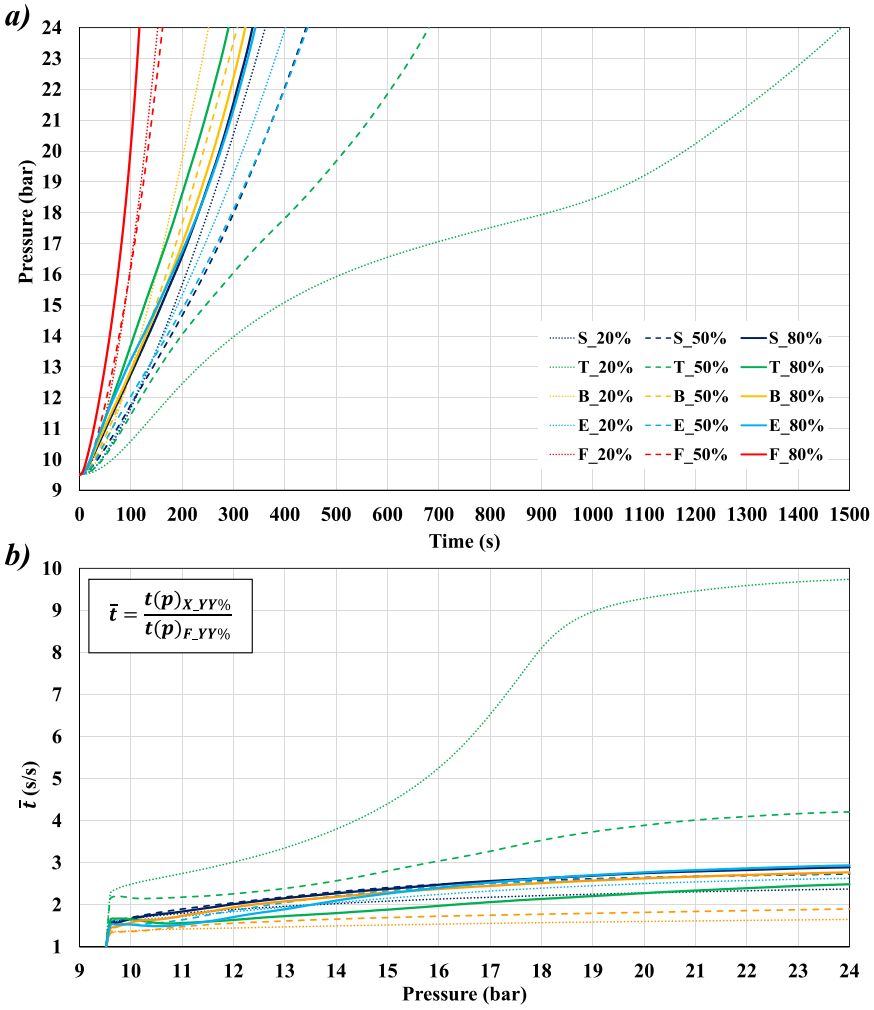

Fig. 3. Pressurization curves (a) and time required to reach a given internal pressure value (b) for all the case studies listed in Table 4.

for most of the cases analyzed. The only exceptions are the T_20% and T_50% cases, requiring a longer time due to the limited areas of the tank surface exposed to the fire in contact with the liquid. Thus, the results obtained show that the rate of pressure increase is not proportional to the percentage of tank surface engulfed in fire. This is confirmed by the bar plot reported in Fig. 4, where panel *a* shows the average pressurization rate for the case studies considered normalized with respect to the corresponding full engulfment case, θ (absolute values of the maximum and average pressurization rates are reported in Table 5), while panel *b* reports the ratio between the surface area of the engulfed zone wetted by the liquid in each case divided by the total surface area of the liquid wetted wall (A_L). Both parameters are evaluated at the beginning of the simulation, i.e. not taking into account the variations deriving from liquid thermal expansion and evaporation.

Most of the values of θ fall between 0.34 and 0.42, and are higher than the value of 0.25 which would be expected in case the pressurization rate was directly proportional to the percentage of tank surface engulfed in fire (which is the same for all case studies). On the other hand, comparing the two panels of Fig. 3, a correlation (yet not linear) can be recognized between the rate of pressurization and the amount of engulfed surface area wetted by the liquid for all the partial engulfment cases with the exception of the E cases. The results reported in Table 5 confirm that tanks with higher degrees of filling show higher values of both maximum and average pressurization rates.

4.2. Accumulation of energy

When a tank containing a liquefied gas under pressure (such as LPG) undergoes catastrophic failure, its content immediately depressurizes to the atmospheric pressure, producing a blast wave due to the sudden vaporization of the liquid and the expansion of the vapor. This phenomenon is referred to as a BLEVE (Boiling Liquid Expanding Vapor Explosion) (Birk et al., 2007; Reid, 1979). The severity of BLEVEs is directly related to the amount of energy stored in the tank lading at the moment of failure (Casal and Salla, 2006; Ogle et al., 2012).

Fig. 5 shows the variation of the internal energy after 120 s of fire exposure for all the partial engulfment cases analyzed, divided by the corresponding value obtained for the full engulfment case.

The effect of the flame zone position is evident. When the fire is impinging on one side (S) or at one end (E) of the tank, the energy accumulation as compared to the full engulfment case is in line with the percentage of outer wall surface area affected by the fire (25% plus the contribution of the transition zone). Conversely, the top and bottom partial engulfment cases show different behaviors. When the flame zone is at the top of the tank, the relative increase in internal energy is much lower (8 to 21% as compared to the corresponding full engulfment case). On the other hand, with the flame zone beneath the tank, the energy accumulated in the lading is up to 50% of that accumulated in the full engulfment case. This is due to the very effective heat transfer mechanism (nucleate boiling) in the liquid phase, which keeps the liquid-wetted wall cool (close to the saturation temperature), ensuring a high

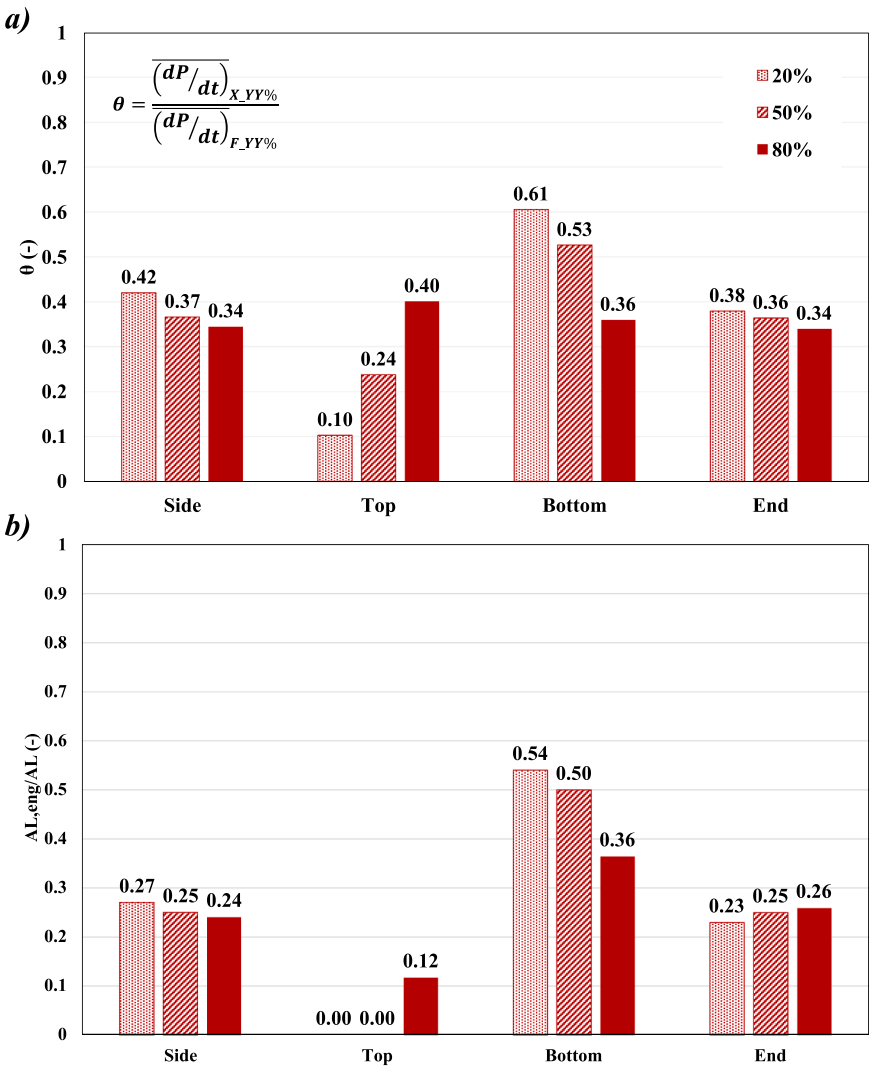

Fig. 4. (a) average pressurization rate normalized with respect to the corresponding full engulfment case for the different partial engulfment scenarios; (b) ratio between the surface area of the engulfed zone wetted by the liquid and the total surface area of the liquid wetted wall, both evaluated at the beginning of the simulation.

Table 5
Maximum and average pressurization rates for all the case studies listed in Table 4.

	Maximum pressurization rate (bar/s)			Average pressurization rate (bar/s)		
	20%	50%	80%	20%	50%	80%
Side	0.058	0.048	0.077	0.040	0.033	0.043
Top	0.019	0.031	0.074	0.010	0.021	0.050
Bottom	0.086	0.064	0.076	0.058	0.047	0.045
End	0.051	0.046	0.073	0.036	0.033	0.042
Full	0.165	0.150	0.274	0.095	0.090	0.125

driving force for the heat transfer (see Eq. 1). On the contrary, as observed in numerous experiment considering different fire scenarios (e.g., Anderson et al., 1974; Birk et al., 2006; Droste and Schoen, 1988; Heymes et al., 2013; Moodie et al., 1988, 1985) the wall section in contact with the vapor heats up rapidly, causing a drop in the driving force. Thus, when the tank is heated from the bottom (B cases), not only is the pressurization higher, but also the accumulation of energy is faster than in the other partial engulfing modes, thus resulting in a more severe BLEVE.

4.3. Temperature transients

Fig. 6 shows the temperature contour plot on the external wall and the symmetry plane after 120 s of fire exposure for all the cases where a 50% filling degree was considered. The temperature difference between the fluid and the wall is evidenced in the Figure. The presence of a temperature gradient is of particular relevance in the liquid phase, which provides a strong cooling effect on the tank wall, efficiently removing the heat from the fire when the flame zone covers regions below the liquid-vapor interface.

The vapor phase shows an important stratification of temperature in all the cases, except for the B_50% case, where the ullage temperature is quite uniform. The liquid phase is stratified as well, but the temperature difference between the warm upper layer in contact with the vapor and the colder core is in the order of a few degrees Celsius, which makes it not visible on the color scale used in Fig. 6. However, due to the strong impact that liquid temperature gradients have on the pressurization rate (especially at high filling levels), the phenomenon of thermal stratification in this phase is discussed in detail in Section 4.5.

4.4. Vessel shell temperatures

The vessel shell temperature is a key factor for vessel integrity in fire

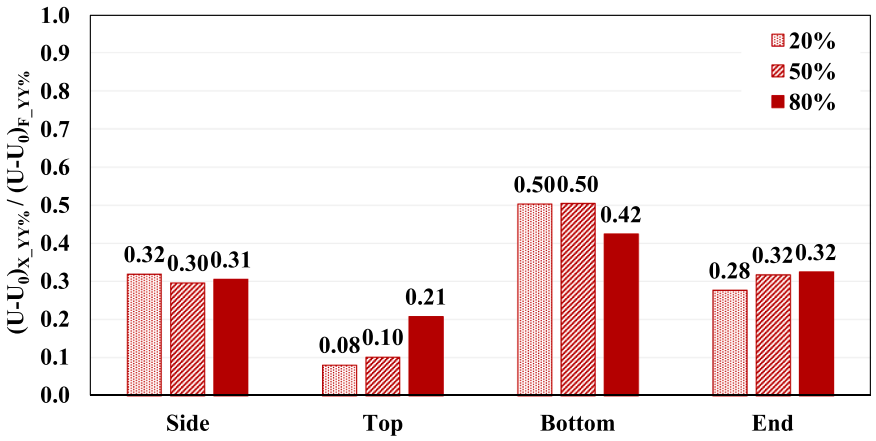

Fig. 5. Variation in the internal energy (U) after 120 s of fire exposure for partial engulfment cases divided by the corresponding value obtained for the full engulfment case.

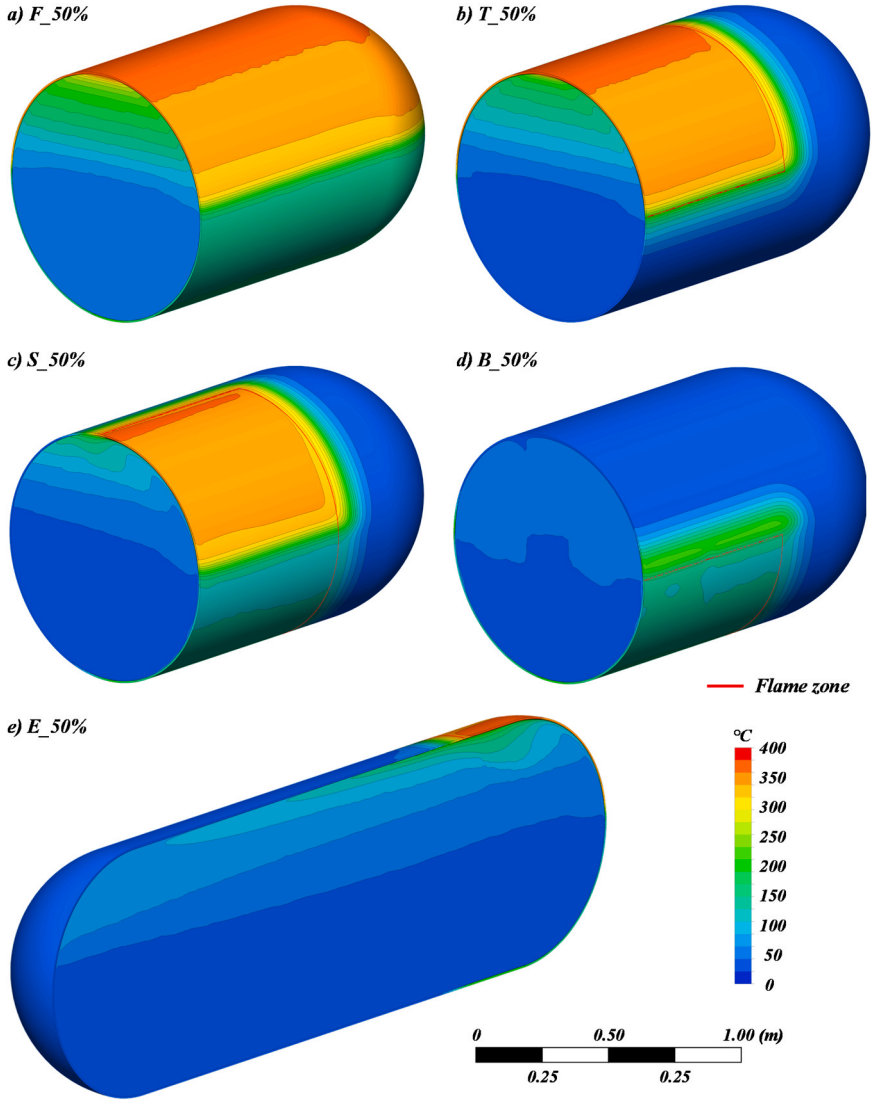

Fig. 6. External wall and symmetry plane temperature contour plots after 120 s of fire exposure for all the cases where a 50% filling degree was considered. The red line highlights the flame zone (not shown in the full engulfment case).

scenarios. The tank structural material, usually carbon steel, suffers a significant reduction in mechanical strength at 400 °C (CEN - European Committee for Standardization, 1998). Above this temperature, creep becomes relevant and the tank wall may experience thinning phenomena that may result in the formation of a crack in the vapor region, which can then propagate and lead to catastrophic failure (Manu et al., 2009). Assessing whether the tank would fail in a specific fire scenario requires a detailed stress analysis (e.g., using finite element methods), which is out of the scope of the present study. However, relevant information concerning tank integrity may be derived from the results reported in Fig. 7.

Fig. 7a shows the maximum wall temperature obtained for all the cases listed in Table 4. Except for the B_50% and B_80% cases, the maximum wall temperature overcomes 400 °C in about 130 s (170 s for the B_20% case) and reaches much higher values by a temperature-time curve that appears to be only weakly influenced by either the engulfment mode and the degree of filling. This is in agreement with both partial and full engulfment fire test results available in the literature (e.g., Birk and VanderSteen, 2006; Moodie et al., 1988). The impact on the mechanical resistance of the tank is visible in Fig. 7b, which shows the time evolution of the ratio between the Von Mises stress in the cylindrical section of the tank, σ_{VM}, and the yield strength, σ_Y, calculated according to Eq. 3:

$$\frac{\sigma_{VM}}{\sigma_Y} = \frac{\frac{p_g \bullet r}{\delta_w}\sqrt{\frac{3}{4}}}{\sigma_{Y,20^\circ C} \bullet k(T_{w,\max})} \tag{3}$$

Where p_g is the gauge pressure in the tank, r is the tank radius, δ_w is the wall thickness, $\sigma_{Y,20^\circ C}$ is the yield strength at ambient temperature (assumed as 240 MPa as common for carbon steel used for pressure tank construction, American Society of Mechanical Engineers, 2019), and k is the strength reduction factor (CEN - European Committee for Standardization, 1998) calculated at the maximum wall temperature $T_{w,max}$. Clearly enough, yielding occurs when σ_{VM}/σ_Y equals 1. According to the results shown in Fig. 7b, it is possible to identify different situations. In full engulfment fire scenarios, the pressure increase is very fast, and the

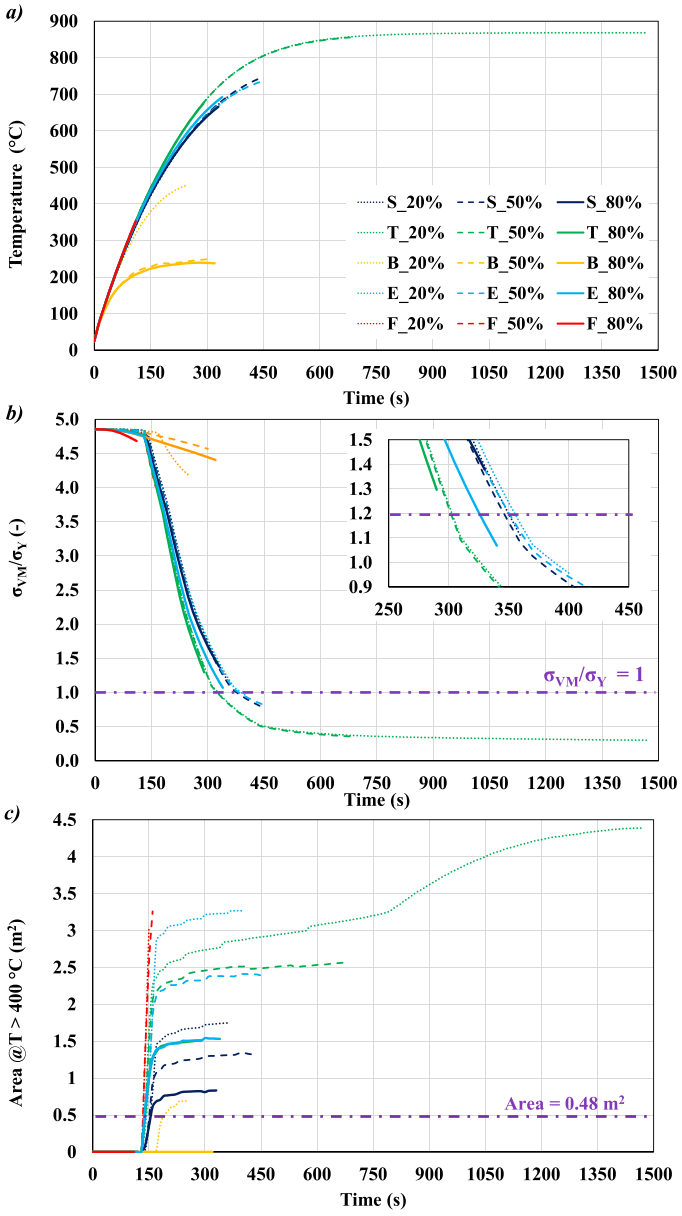

Fig. 7. Maximum wall temperature (a), von Mises stress, σ_{VM}, divided by yield strength, σ_V (b), and shell surface area above 400 °C (c) as a function of time for alla the cases listed in Table 4.

PRV (set point at 24 bar, when the simulations are stopped) opens when the tank is far from the yielding point ($\sigma_{VM}/\sigma_Y >> 1$). On the contrary, when partial engulfment with the flame zone at the top, the side, or the end of the tank is considered, the pressurization is slower, and the wall temperature has enough time to reach values that induce severe mechanical weakening. Thus, the σ_{VM}/σ_Y approaches unity (and in most cases becomes lower than 1) well before the activation of the PRV. The cases where the fire engulfs the bottom part of the tank (B) represent a hybrid condition: the pressurization is slower than in the full engulfment scenario, but the wall temperature increase is slower, so that σ_{VM}/σ_Y is still far from unity when the PRV opens.

Another key factor for the tank integrity under fire exposure is the extension of the zone experiencing mechanical weakening. Using finite element stress rupture analysis, Manu et al. (2009) demonstrated that, for a given peak wall temperature ($T_{w,max}$), higher hot spots result in lower failure time. Fig. 7c shows the extension of the weakened area (here defined as the surface area of the tank outer wall where the temperature is higher than 400 °C) as a function of time for all the cases listed in Table 4. Different from the maximum wall temperature, this parameter is strongly affected by the engulfment mode and the filling degree. It is worth noticing the (positive) cooling effect of the liquid in the cases where an 80% filling degree is considered.

In most of the cases, the extension of the weakened area overcomes 0.48 m^2 (purple dash-dotted line), proposed by Scarponi et al. (2020) as the threshold above which the tank integrity is threatened, based on the experimental work by Birk (2005). Thus, the cases where the fire affects the top or the end of the tank stand out as the most critical partial engulfment scenarios.

4.5. Flow field and thermal stratification

The free convection-driven flow field of the fluid inside the tank, caused by the heat transfer through the vessel shell, has a relevant effect on the fluid temperature and, ultimately, on the pressurization rate of the vessel. The CFD approach developed allows analyzing in detail the local features characterizing the thermo-fluid-dynamic response to the system under investigation.

Fig. 8 shows the streamlines departing from points on the xy plane at 1 cm from the inner wall calculated at an internal pressure value of 19 bar (i.e., twice the initial pressure) for all the cases where an 80%

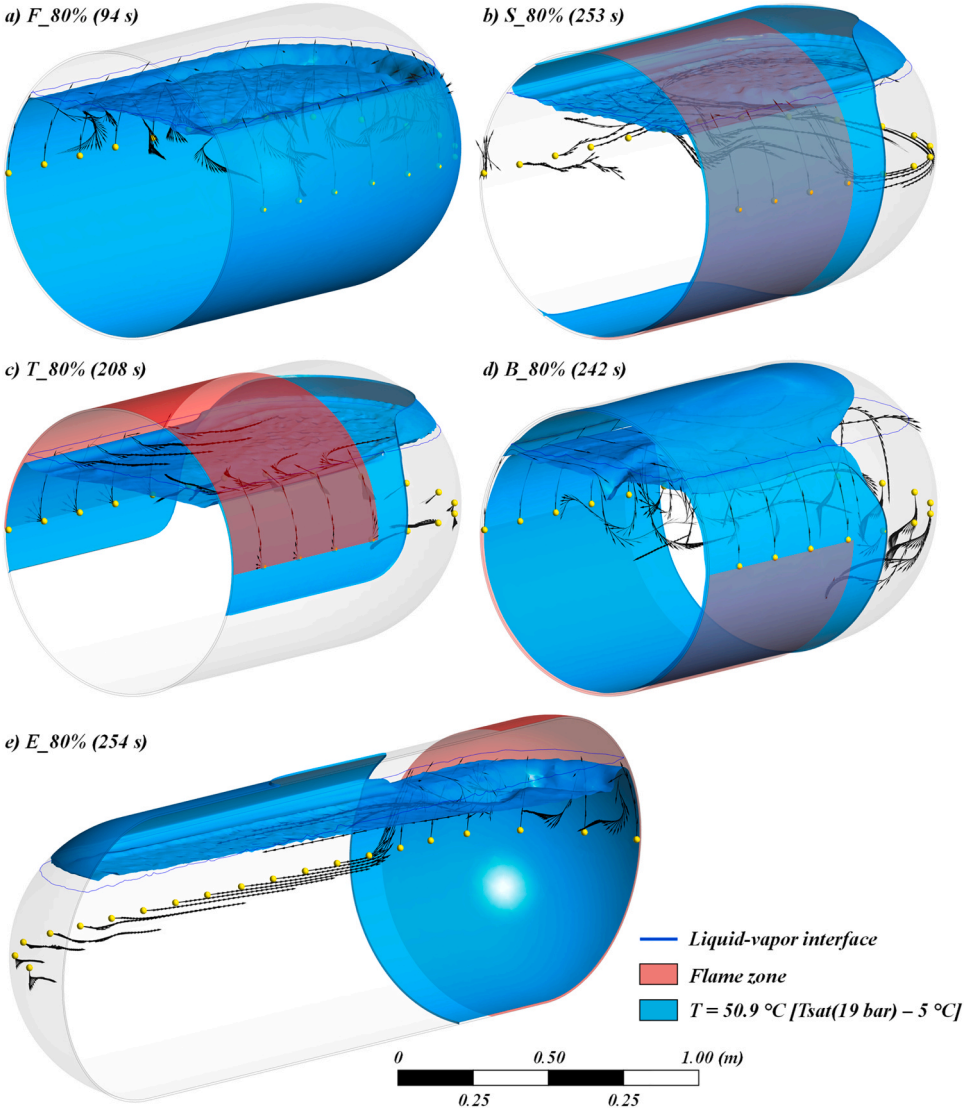

Fig. 8. Streamlines departing from the yellow points equally spaced on the xy plane at 1 cm from the inner wall calculated at a pressure value of 19 bar for all the cases where an 80% filling degree was considered. Vectors composing each streamline are placed at an interval of 0.5 s and extend for a total duration of 15 s. The cyan surface cuts the liquid domain where the temperature equals 50.9 °C (the saturation temperature of the liquid in the tank reduced by 5 °C). The red area indicates the flame zone (not shown in the full engulfment case).

filling degree was considered. As shown in the figure, a free-convective layer develops in correspondence with the flame zone, determining a continuous intake of warm liquid to the region below the liquid-vapor interface. A recirculation flow is thus established, which recalls cold liquid from outside the engulfed zone.

In agreement with experimental observations gathered in full engulfment (Anderson et al., 1974; Moodie et al., 1988) and partial engulfment fire tests (Birk et al., 2006), the liquid stratification phenomenon is well visible in all the scenarios. The cyan surface in Fig. 8 indicates where the temperature equals 50.9° (corresponding to the saturation temperature of the liquid at the tank pressure, reduced by 5 °C), thus providing a visualization of the liquid stratification process. The inhomogeneity that characterizes the system from the thermodynamic point of view is evident as well as the influence that the different engulfment modes have on the spatial distribution of hot and cold zones. Fig. 8 shows that the extension of the warm layer in the liquid phase, which drives the tank pressurization through evaporation, is not limited to the area in the proximity of the engulfed zone. Cold zones where vapor phase condensation occurs are also evident in the figure, above the liquid-vapor interface. These are located in the proximity of the wall, far from the flame zone.

The analysis of the dynamic evolution of thermal stratification for all the cases listed in Table 4 is summarized in Fig. 9, which reports the variation, as a function of time, of the total pressure inside the vessel divided by the saturation pressure of the internal fluid, calculated at the average liquid temperature.

This parameter was proposed by Birk and Cunningham (1996) as a measure of the extension of thermal stratification in tanks exposed to external fires. Values close to unity suggest that the liquid temperature is homogeneous and near saturation, while high values of the ratio indicate a relevant thermal stratification, with most of the liquid phase in a subcooled condition. The latter is the situation observed in all the cases featuring a high degree of filling (i.e., the 80% cases) and when the flame zone is at the top of the tank. Remarkably, the T_80% case shows a degree of thermal stratification comparable with the full engulfment one. On the other hand, the stratification is weaker for the S_50%, B_50, F_50, E_50%, and E_20% cases. The F_20%, B_20%, and S_20% cases exhibit unexpected behavior, with the liquid phase slightly superheated. There is no evidence of this happening in fire tests on LPG tanks with low filling degrees. Thus, these results may be ascribed to an inherent limitation of the VOF approach (in which the liquid and vapor phases share a single temperature value), when coupled with the evaporation and condensation model used in the present study.

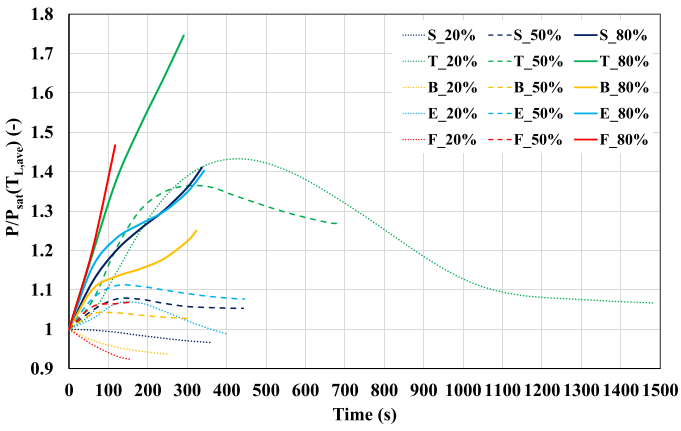

Fig. 9. Time evolution of the tank internal pressure divided by the saturation pressure of the liquid calculated at the average liquid temperature as a function of time for all the cases listed in Table 4.

5. Discussion

The phenomena characterizing the thermo-hydraulic response of pressure vessels to fire exposure are complex and interactive. Thus, predicting pressurization (and ultimately time to failure) is a demanding task. This becomes even more challenging when non-uniform fire conditions are to be analyzed, in which local effects play a major role. The outcomes of the comparative analysis of the case studies listed in Table 4 suggest that both engulfment mode and liquid filling degree have a strong influence on pressurization rate, energy accumulation, and high-temperature mechanical weakening of the tank structure. In particular:

- Except when partial engulfment affects the bottom section of the tanks (B), higher filling degrees promote faster internal pressurization;
- The energy accumulation is faster in the fire scenarios where the flame zone is at the bottom of the tank (maximizing the heat flux to the liquid phase);
- The risk of tank failure due to mechanical weakening is lower when the flame zone affects the bottom of the tank;
- Fire scenarios where the flame zone is at the top or at the end of the tank are particularly critical when the degree of filling is low or medium (e.g., see results obtained for T_20%, T_50%, E_20%, and E_50% cases) due to the extension of the weakened zone.

To the best of the authors' knowledge, experimental data deriving from the systematic study of the effect of the combination of different exposure modes and filling levels are not available in the literature. However, the above considerations are in agreement with experimental evidence collected during different fire test campaigns carried out in the last decades addressing the behavior of LPG tanks at different filling degrees in different fire scenarios, such as full engulfing pool fires (Anderson et al., 1974; Droste and Schoen, 1988; Moodie et al., 1988, 1985), partially engulfing pool fires (Birk et al., 2006) and exposure to distant radiation sources representing wildfires and interface fires (Heymes et al., 2013).

The analysis of the free-convection-driven flow field and temperature distribution highlighted that complex recirculation patterns develop in the tank, promoting thermal stratification of the liquid phase, especially when the filling degree is high. This aspect is of particular importance since lumped models usually adopted in tank integrity studies and in the design of depressurization systems disregard stratification phenomena, possibly providing under-conservative results. An example is reported in Fig. 10, where the pressure curves from the CFD simulations are compared to those calculated by AFFTAC 5.10 (Johnson, 1998a, 1998b; Runnels, 2022), which is a standard tool used for the prediction of the response of tanks to fire exposure and for the assessment of the performance of thermal protection systems in transportation, process and oil&gas applications. It must be remarked that in AFFTAC 5.10 it is not possible to specify the location of the flame zone but only the extension of the area affected by the flame. Thus, for each filling degree considered in the present study, the AFFTAC software was run twice: first assuming full engulfment, and then considering 25% of the outer wall of the tank engulfed in fire. The results are compared to CFD simulations in Fig. 10.

As shown in the Figure, at low filling degrees (Fig. 10a) the lumped model provides conservative predictions with respect to CFD results, regardless of the fire engulfment mode. The same applies to 50% filling degree cases (Fig. 10b), except for the fire scenario where the flame zone affects the bottom of the tank. Completely different results are obtained when the 80% filling degree is considered (Fig. 10c). The lumped model provides lower pressures than the CFD model in these cases. Actually, the pressure obtained from the AFFTAC model is 16.6% (E_80% case) to 26.4% (T_80% case) lower than in CFD simulations when the 80% filling degree is considered. This also results in an overestimation of the time to reach 24 bar (the pressure at the end of CFD simulations) by the AFFTAC

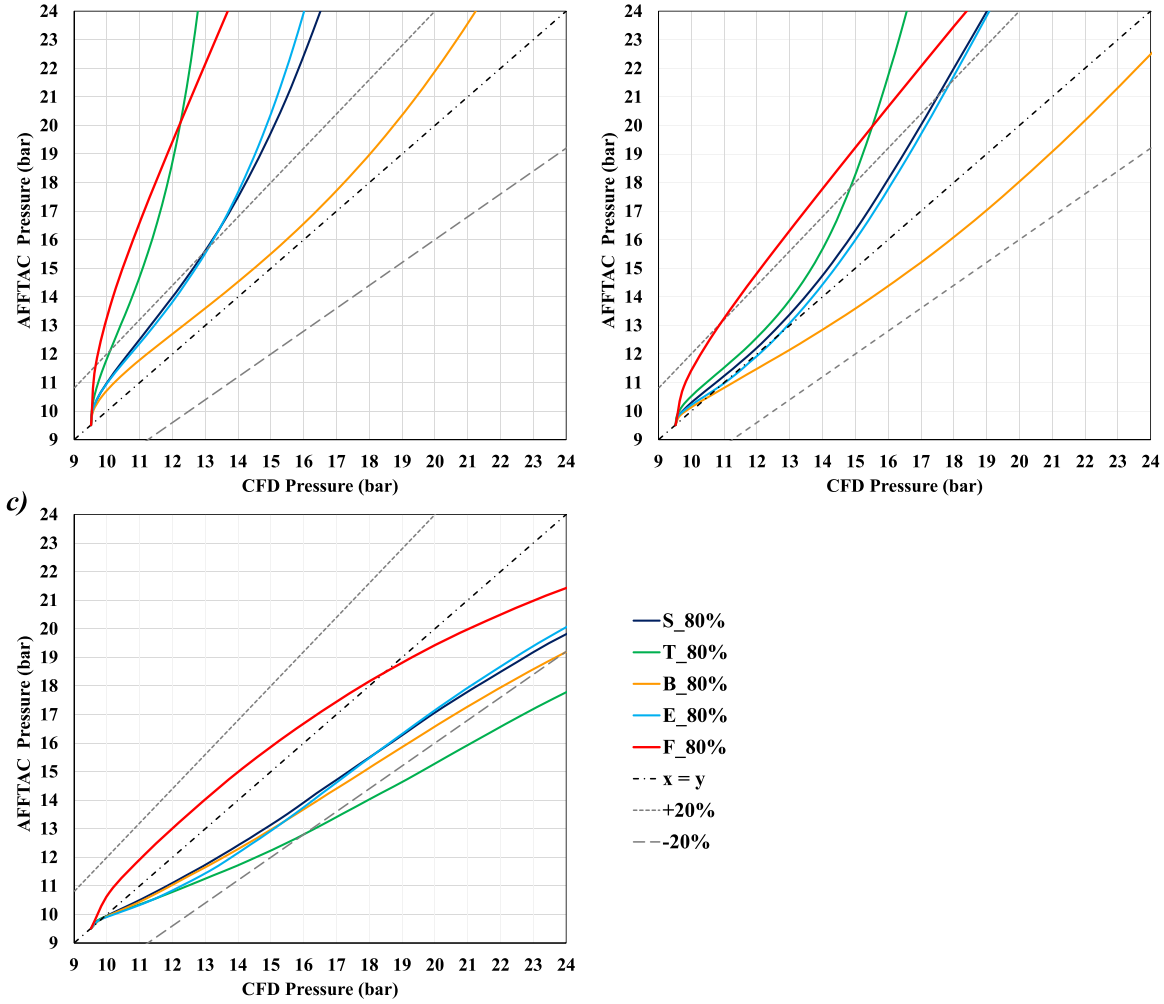

Fig. 10. Parity plots comparing pressure obtained by AFFTAC 5.10 with CFD simulations for 20% filling degree (a), 50% filling degree (b), 80% filling degree (c), and full engulfment cases.

model in these scenarios.

The underestimation of internal pressure, with respect to time, during fire exposure in the AFFTAC model, is caused by the inability of the zone models to capture thermal stratification which, as discussed in Section 4.4, becomes important when the filling degree is high (see Fig. 8 and Fig. 9). It is reasonable to assume that similar results would be obtained by using other lumped models available in the literature that, as the AFFTAC model, neglect thermal stratification. It is also important to remark that the outcomes of experimental and numerical studies on LPG tanks exposed to full-engulfing pool fires (e.g., Hadjisophocleous et al., 1990; Moodie et al., 1988; Scarponi et al., 2018a) highlight that the relevance of this phenomenon increases with the size of the tank.The results obtained are important to highlight how CFD simulations based on a validated approach may be exploited as a "digital twin" of a fire test, overcoming the inherent limitations of large-scale experiments previously highlighted, while preserving an accurate representation of the physical phenomena involved in real scenarios. This paves the way for the investigation of complex aspects that can help to identify the limitations of simplified approaches, proposing sound practical solutions to improve the safety of pressurized tanks (and of other types of industrial equipment) in case of fire. In perspective, the CFD model may be used as a virtual workbench to assess the effectiveness of fire protection systems, such as water deluge systems, depressurization systems, and thermal insulation, also in the presence of defects (e.g., see Scarponi et al., 2017 and Yoon and Birk, 2004).

The computational time stands out as one of the most important drawbacks of the proposed CFD approach. The simulation of 1 s real-time on an Intel® Core™ i9–9940 CPU @ 3.30 GHz using 16 logical processors in parallel required 30 min. Considering that the system analyzed in the present study can be categorized as small with respect to the size range of typical tanks used for full-scale industrial storage and transportation applications, it can be concluded that the modeling approach proposed is not suitable for a rapid assessment of tank response (e.g., as in real-time emergency response). In perspective, the increase in the availability of high-performance computational resources will overcome this issue in the future. Meanwhile, the development of machine learning-based models and/or the extension of the available lumped models based on the results of a limited number of CFD simulations may represent a viable alternative.

Besides computational cost, further issues still need to be thoroughly addressed, the main one being the current lack of CFD approaches able to simulate the tank behavior after the opening of the PRV. Additional research shall explore the integration between CFD simulations and stress analysis of the tank (as in the work by Manu et al., 2009), with the aim of improving the prediction of tank time to failure under fire exposure.

6. Conclusions

The present study proposed a parametric analysis to investigate the behavior of a 1.9 m^3 bullet LPG tank in partial engulfment fire scenarios. A set of case studies was defined varying the positions of the zone

exposed to fire and the filling degree of the tank. These were simulated using a CFD modeling approach previously validated against partial engulfment fire test results. The outcomes of the simulations show that both the engulfment mode and the filling degree have a strong influence on the pressurization rate, energy accumulation, and high-temperature mechanical weakening of the tank structure. The analysis of the simulated flow field highlighted how the development of complex free-convection-driven recirculation patterns promotes thermal stratification, which speeds up the pressure increase.

In case of a fire attack, emergency response teams should prioritize the actions aimed at cooling down the portion of the tank shell above the liquid-vapor interface. This zone shall be monitored with particular attention in order to spot the possible formation of bulges (clear evidence of imminent tank failure) and, in case, the immediate evacuation of emergency teams should be disposed. If depressurization or liquid pull-down systems are in place, they shall continue to operate to minimize the magnitude of possible BLEVE events following tank failure. The application of fireproofing represents a valid mitigation barrier, slowing down pressurization, delaying the accumulation of energy, and keeping at lower temperatures the vapor-wetted wall to prevent high-temperature mechanical weakening.

The comparison of the CFD simulation results to those obtained by using a conventional lumped model that neglects thermal stratification, AFFTAC 5.10, shows that the latter provides non-conservative pressurization curves for all the cases with high filling degrees (80%). A practical solution to obtain conservative results when assessing the response of tanks with a high (> 50%) filling degree exposed to partial engulfment scenarios using lumped models is to consider a full engulfment condition.

Overall, the outcomes of the present study show that a validated CFD approach can be used as a virtual workbench to analyze complex safety-critical scenarios that may be difficult to test experimentally, providing valuable knowledge to improve the safety and integrity of process and storage equipment.

Appendix

Figure A1 provides an overview of the model validation showing the comparison between the model prediction as applied to simulate the partial engulfment fire test carried out on an LPG tank by Birk and co-workers (Birk et al., 2006). The figure evidences that the model results are in good agreement with the experimental data both in terms of pressurization and temperature evolution inside the tank. Further details can be found in Scarponi et al. (2021).

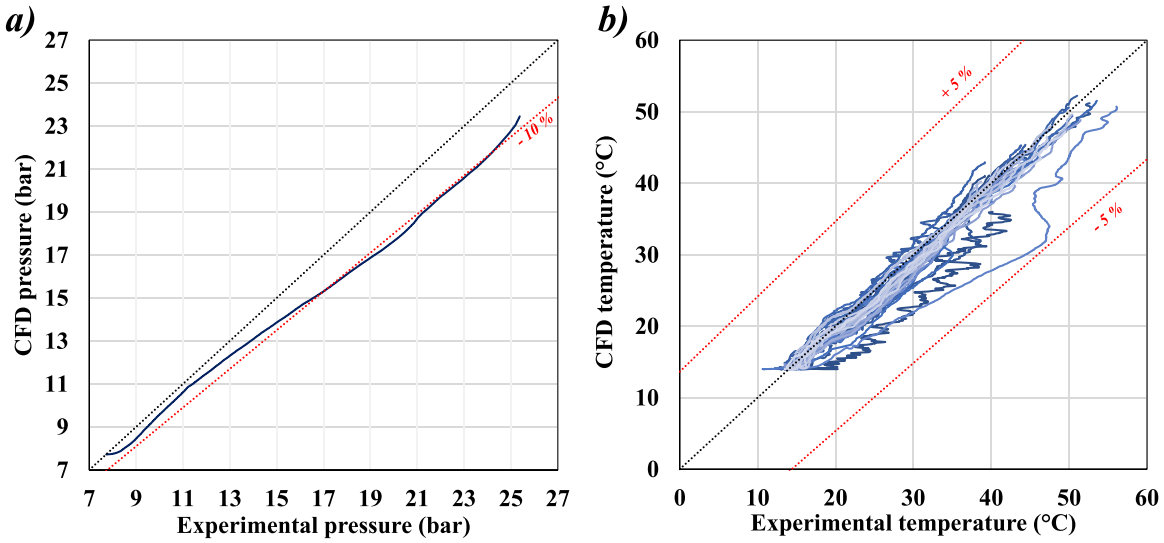

Fig. A1. Comparison of CFD modeling results (Scarponi et al., 2021) and experimental data (Birk et al., 2006) in terms of pressurization (a) and temperature (b) curves.

.

References

American Society of Mechanical Engineers, 2019. ASME Boiler and Pressure Vessel Code An International Code Section II - Part A Ferrous Material Specifications.

Anderson, C., Townsend, W., Zook, J., Cowgill, G., 1974. The effects of a fire environment on a rail tank car filled with LPG. US Dept Trans. Rept No FRA-ORD 31–75.

ANSYS Inc, 2015. ANSYS FLUENT Theory Guide 12.0 Theory Guide, SAS IP, Inc. ANSYS Inc, Cecil Township, PA.

Aydemir, N.U., Magapu, V.K., Sousa, A.C.M., Venart, J.E.S., 1988. Thermal response analysis of LPG tanks exposed to fire. J. Hazard Mater. 20, 239–262. https://doi.org/10.1016/0304-3894(88)87015-8.

Birk, A.M., 2005. Tank-Car Thermal Protection Defect Assessment: Updated Thermal Modelling with Results of Fire Testing.

Birk, A.M., 2006. Fire Testing and Computer Modelling of Rail Tank-Cars Engulfed in Fires: Literature Review.

Birk, A.M., Cunningham, M.H., 1996. Liquid temperature stratification and its effect on BLEVEs and their hazards. J. Hazard Mater. 48, 219–237. https://doi.org/10.1016/0304-3894(95)00157-3.

Birk, A.M., Davison, C., Cunningham, M., 2007. Blast overpressures from medium scale BLEVE tests. J. Loss Prev. Process Ind. 20, 194–206. https://doi.org/10.1016/j.jlp.2007.03.001.

Birk, A.M., Dusserre, G., Heymes, F., 2013. Analysis of a propane sphere BLEVE. Chem. Eng. Trans. 31, 481–486.

Birk, A.M., VanderSteen, J.D.J., 2006. On the transition from non-BLEVE to BLEVE failure for a 1.8m3 propane tank. Trans. ASME 128, 648–655. https://doi.org/10.1115/1.2349579.

Birk, A.M., Poirier, D., Davison, C., 2006. On the response of 500 gal propane tanks to a 25% engulfing fire. J. Loss Prev. Process Ind. 19, 527–541. https://doi.org/10.1016/j.jlp.2005.12.008.

Casal, J., Salla, J.M., 2006. Using liquid superheating energy for a quick estimation of overpressure in BLEVEs and similar explosions. J. Hazard Mater. 137, 1321–1327. https://doi.org/10.1016/j.jhazmat.2006.05.001.

CEN - European Committee for Standardization, 1998. EN 10222–1. Steel forgings for pressure purposes. Part 1: General requirements for open die forgings. European Committee for Standardization, Brussels.

CGSB, 2002. Construction and maintenance of tank car tanks for the transportation of dangerous goods by rail.

Droste, B., Schoen, W., 1988. Full scale fire tests with unprotected and thermal insulated LPG storage tanks. J. Hazard Mater. 20, 41–53. https://doi.org/10.1016/0304-3894(88)87005-5.

Hadjisophocleous, G.V., Sousa, A.C.M., Venart, J.E.S., 1990. A study of the effect of the tank diameter on the thermal stratification in LPG tanks subjected to fire engulfment. J. Hazard Mater. 25, 19–31. https://doi.org/10.1016/0304-3894(90)85067-D.

Heymes, F., Aprin, L., Birk, A.M., Slangen, P., Jarry, J.B., François, H., Dusserre, G., 2013. An experimental study of an LPG tank at low filling level heated by a remote wall fire. J. Loss Prev. Process Ind. 26, 1484–1491. https://doi.org/10.1016/j.jlp.2013.09.015.

Hirt, C.W., Nichols, B.D., 1981. Volume of fluid (VOF) method for the dynamics of free boundaries. J. Comput. Phys. 39, 201–225. https://doi.org/10.1016/0021-9991(81)90145-5.

Johnson, M.R., 1998a. Tank car thermal analysis, volume 1, user's manual for analysis program, DOT/FRA/ORD-98/09A. Department of Transportation, Federal Railroad Administration, Washington DC.

Johnson, M.R., 1998b. Tank car thermal analysis, Volume 2, Technical Documentation Report for Analysis Program. US Department of Transportation, Federal Railroad Administration, Washington DC.

Kamperveen, J.P., Spruijt, M.P.N., Reinders, J.E.A., 2016. Heat load resistance of cryogenic storage tanks-results of LNG safety program. Utrecht: TNO.

Lee, W.H., 1979. A pressure iteration scheme for two-phase modeling technical report LA-UR 79–975. Los Alamos, New Mexico.

Liley, P.E., Thomson, G.H., Friend, D.G., Daubert, T.E., Buck, E., 1999. Physical and chemical data, Section 2, in: Perry's Chemical Engineers' Handbook. McGraw Hill, New York, NY.

Malm, S., 2018. New CCTV shows moment gas tanker plowed into back of a truck, sparking explosion that left one dead and scores injured in Italy. MailOnline.

Mannan, S., 2012. Lees' loss prevention in the process industries: hazard identification. Assessment and Control, fourth ed. Elsevier, Oxford (UK).

Manu, C.C., Birk, A.M., Kim, I.Y., 2009. Stress rupture predictions of pressure vessels exposed to fully engulfing and local impingement accidental fire heat loads. Eng. Fail Anal. 16, 1141–1152.

Moodie, K., 1988. Experiment and modelling:- an overiview with particular reference to fire engulfment. J. Hazard Mater. 20, 149–175. https://doi.org/10.1016/0304-3894(88)87011-0.

Moodie, K., Billinge, K., Cutler, D.P., 1985. The fire engulfment of LPG storage tanks. IChemE Symp. (93), 87–106.

Moodie, K., Cowley, L.T.T., Denny, R.B.B., Small, L.M.M., Williams, I., 1988. Fire engulfment tests on a 5 tonne LPG tank. J. Hazard Mater. 20, 55–71. https://doi.org/10.1016/0304-3894(88)87006-7.

Ogle, A.R., Ramirez, J.C., Smyth, S.A., 2012. Calculating the explosion energy of a boiling liquid expanding vapor explosion using exergy analysis. Process Saf. Prog. 31, 51–54. https://doi.org/10.1002/prs.

Planas, E., Pastor, E., Casal, J., Bonilla, J.M., 2015. Analysis of the boiling liquid expanding vapor explosion (BLEVE) of a liquefied natural gas road tanker: the zarzalico accident. J. Loss Prev. Process Ind. 34, 127–138. https://doi.org/10.1016/J.JLP.2015.01.026.

Planas-Cuchi, E., Gasulla, N., Ventosa, A., Casal, J., 2004. Explosion of a road tanker containing liquified natural gas. J. Loss Prev. Process Ind. 17, 315–321. https://doi.org/10.1016/J.JLP.2004.05.005.

Reid, R.C.C., 1979. Possible mechanism for pressurized-liquid tank explosions or BLEVE's. Science 203 (1979), 1263–1265. https://doi.org/10.1126/science.203.4386.1263.

Reniers, G., Cozzani, V., 2013. Domino effects in the process industries: modelling. Prevention and Managing, Domino Effects in the Process Industries: Modelling, Prevention and Managing. Elsevier B.V. https://doi.org/10.1016/C2011-0-00004-2.

Ricci, F., Scarponi, G.E., Landucci, G., Cozzani, V., 2021. Fire driven domino effect. In: Khan, F., Cozzani, V., Reniers, G. (Eds.), Domino Effect: Its Prediction and Prevention, Methods in Chemical Process Safety. Elsevier, pp. 71–117. https://doi.org/10.1016/bs.mcps.2021.05.003.

Runnels, S.R., 2022. AFFTAC.

Scarponi, G.E., Bradley, I., Landucci, G., Birk, A.M., Cozzani, V., 2022. Modelling pressure tanks under fire exposure: past experience. Curr. Chall. Future Perspect. Chem. Eng. Trans. 90, 481–486. https://doi.org/10.3303/CET2290081.

Scarponi, G.E., Landucci, G., Birk, A.M., Cozzani, V., 2018a. LPG vessels exposed to fire: scale effects on pressure build-up. J. Loss Prev. Process Ind. 56, 342–358. https://doi.org/10.1016/j.jlp.2018.09.015.

Scarponi, G.E., Landucci, G., Birk, A.M., Cozzani, V., 2019. An innovative three-dimensional approach for the simulation of pressure vessels exposed to fire. J. Loss Prev. Process Ind. 61, 160–173. https://doi.org/10.1016/j.jlp.2019.06.008.

Scarponi, G.E., Landucci, G., Birk, A.M., Cozzani, V., 2021. Three dimensional CFD simulation of LPG tanks exposed to partially engulfing pool fires. Process Saf. Environ. Prot. 150, 385–399. https://doi.org/10.1016/j.psep.2021.04.026.

Scarponi, G.E., Landucci, G., Heymes, F., Cozzani, V., 2018b. Experimental and numerical study of the behavior of LPG tanks exposed to wildland fires. Process Saf. Environ. Prot. 114, 251–270. https://doi.org/10.1016/j.psep.2017.12.013.

Scarponi, G.E., Landucci, G., Tugnoli, A., Cozzani, V., Birk, A.M., 2017. Performance assessment of thermal protection coatings of hazardous material tankers in the presence of defects. Process Saf. Environ. Prot. 105, 393–409. https://doi.org/10.1016/j.psep.2016.10.009.

Scarponi, G.E., Pastor, E., Planas, E., Cozzani, V., 2020. Analysis of the impact of wildland-urban-interface fires on LPG domestic tanks. Saf. Sci. 124, 104588 https://doi.org/10.1016/j.ssci.2019.104588.

van Wingerden, K., Kluge, M., Habib, A.K., Ustolin, F., Paltrinieri, N., 2022. Medium-scale tests to investigate the possibility and effects of BLEVEs of storage vessels containing liquified hydrogen. Chem. Eng. Trans. 90. https://doi.org/10.3303/CET2290092.

Wang, J., Chen, X., Li, Y., Wang, M., Yu, X., Zong, R., Lu, S., 2022a. Effects of filling level and tray size on the burning behavior of a tank during burning of leaking contents: An integrated experimental and numerical approach. Process Saf. Environ. Prot. 168, 513–525. https://doi.org/10.1016/J.PSEP.2022.10.018.

Wang, J., Wang, M., Yu, X., Zong, R., Lu, S., 2022b. Experimental and numerical study of the fire behavior of a tank with oil leaking and burning. Process Saf. Environ. Prot. 159, 1203–1214. https://doi.org/10.1016/J.PSEP.2022.01.047.

Wang, M., Wang, J., Yu, X., Zong, R., 2023. Experimental and numerical study of the thermal response of a diesel fuel tank exposed to fire impingement. Appl. Therm. Eng. 227, 120334 https://doi.org/10.1016/J.APPLTHERMALENG.2023.120334.

Yoon, K.T., Birk, A.M., 2004. Computational Fluid Dynamics Analysis of Local Heating of Propane Tanks.